



Contents lists available at ScienceDirect

# Bioorganic & Medicinal Chemistry Letters

journal homepage: [www.elsevier.com/locate/bmcl](http://www.elsevier.com/locate/bmcl)

## Discovery of triazine-benzimidazoles as selective inhibitors of mTOR

Emily A. Peterson<sup>a,\*</sup>, Paul S. Andrews<sup>b</sup>, Xuhai Be<sup>c</sup>, Alessandro A. Boezio<sup>a</sup>, Tammy L. Bush<sup>d</sup>, Alan C. Cheng<sup>e</sup>, James R. Coats<sup>a</sup>, Adria E. Colletti<sup>c</sup>, Katrina W. Copeland<sup>a</sup>, Michelle DuPont<sup>d</sup>, Russell Graceffa<sup>a</sup>, Barbara Grubinska<sup>d</sup>, Jean-Christophe Harmange<sup>a,†</sup>, Joseph L. Kim<sup>f</sup>, Erin L. Mullady<sup>b</sup>, Philip Olivieri<sup>a</sup>, Laurie B. Schenkel<sup>a</sup>, Mary K. Stanton<sup>g</sup>, Yohannes Teffera<sup>e</sup>, Douglas A. Whittington<sup>f</sup>, Ti Cai<sup>d</sup>, Daniel S. La<sup>a,\*</sup>

<sup>a</sup> Medicinal Chemistry, Amgen Inc., 360 Binney St., Cambridge, MA 02142, USA<sup>b</sup> Lead Discovery, Amgen Inc., 360 Binney St., Cambridge, MA 02142, USA<sup>c</sup> Pharmacokinetics and Drug Metabolism, Amgen Inc., 360 Binney St. Cambridge, MA 02142, USA<sup>d</sup> Oncology Research, Amgen Inc., 360 Binney St., Cambridge, MA 02142, USA<sup>e</sup> Molecular Structure, Amgen Inc., 1120 Veterans Blvd., South San Francisco, CA 94080, USA<sup>f</sup> Molecular Structure, Amgen Inc., 360 Binney St. Cambridge, MA 02142, USA<sup>g</sup> Pharmaceuticals R&D, Amgen Inc., 360 Binney St., Cambridge, MA 02142, USA

### ARTICLE INFO

#### Article history:

Received 7 December 2010

Revised 28 January 2011

Accepted 2 February 2011

Available online 12 February 2011

#### Keywords:

mTOR

Kinase inhibitor

Oncology

Benzimidazole

Triazine

### ABSTRACT

mTOR is part of the PI3K/AKT pathway and is a central regulator of cell growth and survival. Since many cancers display mutations linked to the mTOR signaling pathway, mTOR has emerged as an important target for oncology therapy. Herein, we report the discovery of triazine benzimidazole inhibitors that inhibit mTOR kinase activity with up to 200-fold selectivity over the structurally homologous kinase PI3K $\alpha$ . When tested in a panel of cancer cell lines displaying various mutations, a selective inhibitor from this series inhibited cellular proliferation with a mean IC<sub>50</sub> of 0.41  $\mu$ M. Lead compound **42** demonstrated up to 83% inhibition of mTOR substrate phosphorylation in a murine pharmacodynamic model.

© 2011 Elsevier Ltd. All rights reserved.

The mammalian target of rapamycin (mTOR) kinase has been identified as a critical signaling node in the promotion of cancer cell growth and survival. mTOR senses the cellular availability of nutrients and energy, serves as a downstream regulator of growth factor signaling, and is ultimately responsible for mediating cell functions such as apoptosis, autophagy, translation, cell cycle regulation, and cytoskeleton reorganization.<sup>1</sup> mTOR functions through two distinct multi-protein complexes, mTOR complex 1 (mTORC1) and mTOR complex 2 (mTORC2). Each complex is defined by its interaction with either Raptor (regulatory-associated protein of mTOR) as in the case of mTORC1 or Rictor (rapamycin-insensitive companion of mTOR) as in the case with mTORC2.

Both complexes play critical roles in the PI3K/AKT cascade, a pathway wherein mutations within its signaling components are frequently present in cancer cells. Mechanistically, PI3K/AKT pathway initiation occurs through activation of receptor tyrosine ki-

nases (RTKs) leading to association with the adaptor protein IRS1 (insulin receptor substrate 1). IRS1 recruits PI3K $\alpha$  to the cell membrane, which converts membrane bound phosphatidylinositol-4, 5-bisphosphate (PIP2) to phosphatidylinositol-3,4,5-trisphosphate (PIP3). PIP3 causes translocation of AKT as well as PDK1 to the cell membrane through association with the conserved pleckstrin homology domain on both proteins. This event leads to the phosphorylation of AKT by PDK1 at the T308 site. Fully activated AKT is generated upon the phosphorylation at S473 by mTORC2. AKT phosphorylates several proximal substrates including PRAS40 and TSC2.<sup>2</sup> Both of these events lead to activation of mTORC1, which phosphorylates 4EBP1 and S6K, integral participants in protein translation and cell growth. mTOR activation also occurs in response to elevated nutrient or amino acid levels through RAG GTPase activation as well as the Ras/Raf/MAPK pathway.<sup>3</sup> Increased activity through any of these mechanisms can lead to increased signaling through mTOR and ultimately unregulated cell growth. Recently, rapamycin and its analogs, which are allosteric inhibitors of mTORC1 exclusively, have received much attention as cancer therapeutics. Efforts in this arena have culminated in the approval of Afinitor® (Everolimus)<sup>4</sup> and Torisel® (Temsirolimus)<sup>5</sup> for renal cell carcinoma. As a result of mTORC1 inhibition,

\* Corresponding authors. Tel.: +1 617 444 5027, fax: +1 617 621 3907 (E.A.P.); tel.: +1 617 444 5189, fax: +1 617 621 3908 (D.S.L.).

E-mail addresses: [epeterso@amgen.com](mailto:epeterso@amgen.com) (E.A. Peterson), [daniel.la@amgen.com](mailto:daniel.la@amgen.com) (D.S. La).

<sup>†</sup> Currently at Constellation Pharmaceuticals, 215 First St., Suite 200, Cambridge MA 02142, USA

rapamycin disrupts the regulating negative feedback loop, which involves the destabilization of IRS1 protein by S6K phosphorylation. The suppression of this feedback mechanism, leading to increased signaling through the PI3K/AKT pathway, could present a liability as increased pAKT levels have been observed in patients treated with rapamycin.<sup>6</sup> Therefore, discovery of an ATP competitive inhibitor, which would target both mTOR complexes through inhibition of mTOR kinase activity, is an attractive approach to preventing the increased AKT signaling produced by exclusive inhibition of mTORC1.<sup>7</sup> Furthermore, it is expected that an mTOR selective inhibitor would demonstrate increased tolerability over a dual PI3K/mTOR inhibitor due to the effects of PI3K inhibition on glucose homeostasis and insulin resistance. In the area of ATP-competitive mTOR selective inhibitors, several compounds have entered the clinic, including AZD8055<sup>8</sup> and OSI-027.<sup>9</sup> Accordingly, as part of our oncology portfolio, we endeavored to develop a selective small molecule inhibitor of mTOR.

Our effort to develop a new class of selective mTOR kinase inhibitors began with a high-throughput screen of our compound collection. A promising hit that emerged from the screening campaign was triazine benzimidazole **1** (Fig. 1A), which inhibited phosphorylation of mTOR substrate 4EBP1 in a Lantha-Screen enzyme assay with an  $IC_{50}$  = 97 nM. It was also moderately potent in two U-87 cellular assays that measure the phosphorylation of 4EBP1 (at T37/46, downstream of mTORC1) and AKT (at S473, which is downstream of mTORC2). As mentioned above, a goal for our program was to develop an mTOR selective inhibitor, which is challenging due to the significant homology between the active site and kinase domains of mTOR and the class I PI3Ks ( $\alpha$ ,  $\beta$ ,  $\delta$ , and  $\gamma$ ). Inhibitor **1** demonstrated modest (3 $\times$ ) selectivity over PI3K $\alpha$ , and when profiled in a binding assay (Ambit) against a panel of 402 kinases, was also found to bind kinases in the Raf pathway as well as KDR, TGFBR2 and DCAMKL3 at [1  $\mu$ M]. Herein we describe the design, structure–activity relationships (SAR), and in vivo profile of selective mTOR inhibitors arising from the initial discovery of benzimidazole triazine **1**.

Due in part to the large size of the mTOR protein (289 kDa), solving a crystal structure of the mTOR kinase domain has been a challenge to the field. However, due to the high homology between mTOR and PI3K $\gamma$  within the ATP binding site, the crystal structure of the kinase domain of PI3K $\gamma$  could provide insight into how inhibitor **1** binds to the mTOR active site. A co-crystal structure of **1** in the kinase domain of PI3K $\gamma$  was obtained and showed that there are several important contacts that compound **1** makes within the ATP binding site of PI3K $\gamma$  (Fig. 1B).<sup>10</sup> Of particular importance is a dual hydrogen bonding interaction between the triazine amine and Val882 (also known as the linker or hinge residue) and the displacement by the phenol of a structural water molecule that bridges Asp841 and Tyr867 in the area known as

the affinity pocket.<sup>11</sup> These interactions are likely similar to those within the mTOR ATP binding domain, since the residues making these interactions are conserved between mTOR and PI3K $\gamma$ . A model of the mTOR kinase domain based on sequence homology with PI3K $\gamma$  was developed to potentially gain a better understanding of the mTOR ATP binding site. The residues labeled in blue are those that are predicted to be different in the mTOR active site, which we hoped to exploit in the development of a selective mTOR inhibitor (Fig. 1B).

Further insight was obtained by inspection of a surface representation of PI3K $\gamma$  bound to **1**, which revealed a small pocket adjacent to the triazine (Fig. 1C, highlighted in yellow). The presence of this extra space and the adjacent tyrosine residue differentiates the mTOR and PIKK kinases from the majority of other protein kinases, which generally contain a carbonyl group that fills this pocket and often interacts with kinase inhibitors through a hydrogen bonding interaction.<sup>12</sup> We therefore investigated substitution of the R<sup>1</sup> position of the triazine linker-binder as a means to provide selectivity over kinases outside the PIKK family (Table 1). Lead compound **1** was modified to analog **10** (R<sup>1</sup> = methyl) and evaluated in a panel of 48 kinases revealing that this small modification removed off-target kinase activity and improved the potency on mTOR (Table 1A). Selectivity over PI3K $\alpha$ , however, remained a challenge. Expansion of the R<sup>1</sup> position to groups larger than methyl (**12**, **13**, and **16**) led to a significant decrease in potency, which is consistent with the limited volume of the pocket adjacent to Tyr867.

A variety of triazine analogs were synthesized and screened with the aim of improving potency and selectivity (Table 1B). Attempts to replace the methyl acetonitrile group with aromatic, benzylic or small alkyl groups lead to decreased potency (**2–5**). Removal or replacement of the R<sup>2</sup> amine also led to inactive compounds (**7** and **8**). The only modification that improved potency was removal of the methylacetonitrile group to give triazine amine **6**. Changing the triazine to a pyrimidine (**11**, X = N  $\rightarrow$  **14**, X = CH) was also investigated but provided no additional improvement in potency or selectivity over PI3K $\alpha$ . Consideration of the SAR developed in Table 1B revealed that methyl aminotriazine **11** was the optimal linker-binder element. Inhibitor **11** was evaluated against a custom panel of 100 kinases to understand its broader selectivity profile. This effort revealed that **11** also demonstrated selectivity for mTOR and the PIKK kinases with the exception of FLT3 (POC = 14) and CSNK2A1 (POC = 15) at [1  $\mu$ M].

The representative route used to synthesize the triazine-benzimidazole compounds is illustrated in Scheme 1, as exemplified by the synthesis of **11**. Methylation of cyanuric chloride (**17**) with methyl magnesium bromide provided methyl dichlorotriazine **18**, which underwent subsequent S<sub>N</sub>Ar displacement with 2-chlorobenzimidazole (**19**). Amination of the remaining chloride on the triazine installed the linker-binding moiety and provided the

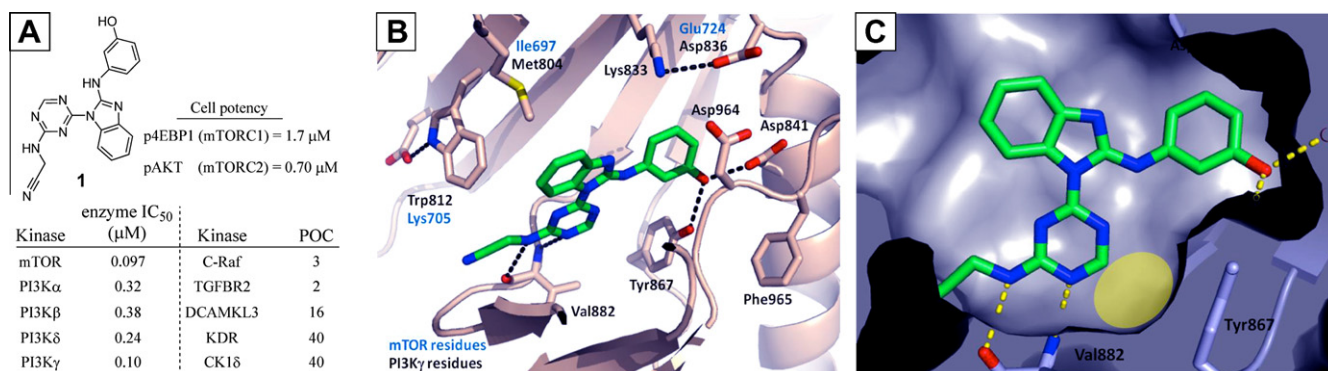
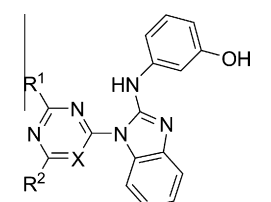


**Figure 1.** (A) HTS hit **1**; (B) co-crystal structure of **1** with PI3K $\gamma$ ; (C) surface representation of PI3K $\gamma$  bound to **1**.

**Table 1**

Modification of the linker-binder moiety provides broader kinase selectivity and improved potency



Compd	C-RAF	KDR	CK1δ	FGFR1
<b>A. Broader kinase selectivity (POC)<sup>a</sup></b>				
<b>1</b>	3	40	40	43
<b>10</b>	92	100	90	100

Compd	R <sup>1</sup>	R <sup>2</sup>	X	mTOR <sup>b</sup>	p4EBP1 <sup>c</sup>	pAKT <sup>d</sup>	PI3Kα <sup>e</sup>
<b>B. Potency on mTOR and selectivity over PI3Kα (IC<sub>50</sub>, μM)</b>							
<b>1</b>	H	NHCH <sub>2</sub> CN	N	0.097	1.7	0.70	0.32
<b>2</b>	H	NHPh	N	2.3	>25	0.87	0.72
<b>3</b>	H	NHMe	N	0.25	2.9	0.18	0.19
<b>4</b>	H	NH <sub>2</sub> CH <sub>2</sub> CF <sub>3</sub>	N	>50	>25	3.2	3.6
<b>5</b>	H	NHCH <sub>2</sub> -2-pyr	N	21	>25	2.4	3.6
<b>6</b>	H	NH <sub>2</sub>	N	0.021	0.71	0.034	0.13
<b>7</b>	H	H	N	3.0	>25	1.6	2.0
<b>8</b>	H	OMe	N	>50	>25	1.9	1.7
<b>9</b>	H	NH <sub>2</sub>	CH	0.11	3.5	0.42	1.0
<b>10</b>	Me	NHCH <sub>2</sub> CN	N	0.008	0.38	0.017	0.032
<b>11</b>	Me	NH <sub>2</sub>	N	0.007	0.15	0.009	0.004
<b>12</b>	Et	NH <sub>2</sub>	N	0.39	6.3	0.41	0.34
<b>13</b>	n-Pr	NH <sub>2</sub>	N	4.7	>25	2.64	3.5
<b>14</b>	Me	NH <sub>2</sub>	CH	0.087	1.2	0.043	0.042
<b>15</b>	Me	H	CH	0.37	8.9	0.60	0.37
<b>16</b>	OMe	NHCH <sub>2</sub> CN	N	>50	21.5	2.1	0.52

<sup>a</sup> Kinase binding assay, POC = % of control at [1 μM].

<sup>b</sup> Inhibition of kinase activity (Lantha-Screen).

<sup>c</sup> Cell assay measuring p4EBP1 in U87 cells.

<sup>d</sup> Cell assay measuring pAKT (S473) in U87 cells.

<sup>e</sup> Inhibition of kinase activity (Alpha-screen).

benzimidazole chloride intermediate **21** (R = H), from which divergent SAR exploration of the affinity pocket could be easily achieved by S<sub>N</sub>Ar displacement. For compound **11**, 3-aminophenol reacted exclusively at the aniline amine upon microwave heating at 140 °C in 2-butanol.

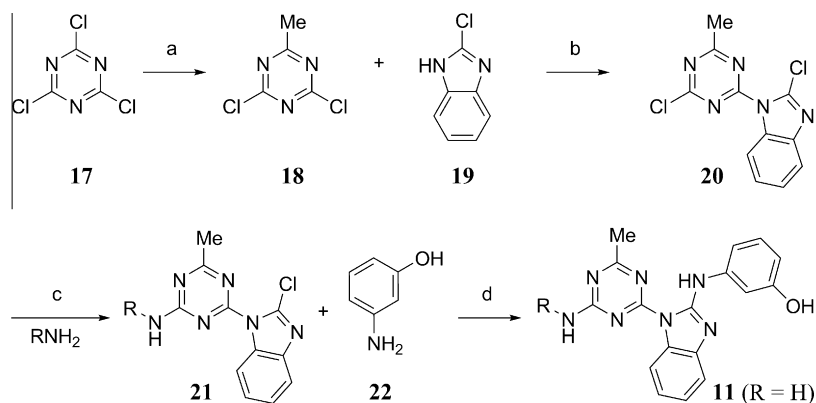
Using the synthesis described for **11** in Scheme 1, which incorporates the affinity pocket moiety as the last step, a wide variety of phenol replacements could be investigated in a rapid fashion with the aim of improving potency against mTOR and selectivity over the PI3Kα, β, δ, and γ isoforms (Table 2). The affinity pocket region within the ATP binding site is a carboxylate-rich region that also

contains the catalytic lysine (Fig. 1B). We therefore anticipated that a polar substituent would be favored, as demonstrated by the diminished mTOR potency for phenyl compound **24** (Table 2). The most potent inhibitor of mTOR in this series was bis-phenol **25**, which also had sub-nanomolar potency on three of the PI3K isoforms. In seeking to replace the phenol group, which could potentially pose a pharmacokinetic liability, several phenol bioisosteres were tested with varying results. While the more traditional carboxamide phenol bioisostere<sup>13</sup> **26** proved to be less potent than the parent phenol, N-linked amides and ureas in the para position were potent although non-selective (**27** and **28**). In general, it was found that arenes attached through a six-membered ring demonstrated excellent potency, but were not selective against PI3Kα.

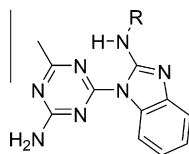
Further investigation revealed that substituting five-membered ring heterocycles for the affinity pocket moiety provided potent inhibitors of mTOR that were moderately selective for mTOR over PI3Kα. The compound that demonstrated the best combination of potency and selectivity was pyrazole **32**, which had an IC<sub>50</sub> of 27 nM for the inhibition of mTOR, was 30-fold selective over PI3Kα, and demonstrated up to 32× selectivity over the other PI3K isoforms. Substitution on the carbons of the pyrazole ring led to a significant decrease in mTOR potency, with the exception of indazole **36**, which demonstrated diminished potency in the p4EBP1 cellular assay. Alkylation of the pyrazole nitrogen was also detrimental (**33**, **34**, and **38**) as was substitution with other related heterocycles such as isoxazole **35** and isothiazole (not shown). In addition, migration of the pyrazole nitrogens to give 4-pyrazolyl isomer **37** or five-membered heterocycles bearing three heteroatoms such as triazole or oxadiazole reduced the potency, as exemplified by **40**.

More drastic changes to the affinity pocket region of the molecule were not tolerated. Replacing the NH linkage between the benzimidazole ring and the affinity pocket moiety with an oxygen or sulfur resulted in IC<sub>50</sub>'s >25 μM. An intramolecular hydrogen bond exists between the NH at the 2-benzimidazole position and the proximal nitrogen on the triazine ring. This interaction is essential for maintaining co-planarity of the triazine and benzimidazole rings, which appears to be a requirement for potency on mTOR. It was also found that only planar, aromatic groups in the affinity pocket resulted in potent inhibition of mTOR, as attachment of alkyl rings, chains, benzyl groups, amides or ureas gave significantly less potent compounds, as exemplified by **41**.

Analysis of the co-crystal structure of pyrazole **32** in the PI3Kγ active site revealed that the pyrazole resided within hydrogen bonding distance of the catalytic Asp836 and Lys833 residues in PI3Kγ (Fig. 2). A key difference in the mTOR active site based on



**Scheme 1.** Synthesis of inhibitor **11**. Reagents and conditions: (a) MeMgBr, Et<sub>2</sub>O/THF, −78 °C to rt (85%); (b) <sup>i</sup>Pr<sub>2</sub>EtN, 1,4-dioxane (55%); (c) 7 N NH<sub>3</sub> in MeOH, rt (90%); (d) 2-butanol, microwave, 140 °C (70%).

**Table 2**  
Modification of the affinity pocket

Compd	R	IC <sub>50</sub> (μm)				
		mTOR <sup>a</sup>	4EBP1 <sup>b</sup>	pAKT <sup>c</sup>	P13Kα <sup>d</sup>	P13Kβ/δ/γ
23		0.007	0.15	0.009	0.004	0.009/0.003/0.008
24		0.42	>25	0.19	0.26	1.0/0.36/0.47
25		0.0002	0.097	0.005	0.0006	0.0002/0.0004/0.005
26		0.175	3.9	0.19	0.29	1.03/0.040/0.48
27		0.002	0.34	0.011	0.006	0.017/0.011/0.013
28		0.013	0.34	0.18	0.023	0.41/0.071/0.02
29		0.29	1.5	0.12	0.63	1.4/0.89/0.11
30		0.028	0.96	0.14	0.23	1.0/0.24/0.34
31		0.027	1.5	0.12	0.20	0.63/0.32/0.20
32		0.027	0.39	0.055	0.80	0.87/0.51/0.32
33		0.27	5.3	0.58	6.2	28.8/4.6/4.1
34		0.34	6.5	0.77	10.4	22.3/0.53/0.86
35		0.15	3.3	0.26	0.84	3.1/1.3/2.3
36		0.06	4.2	0.25	0.96	0.42/0.27/0.19
37		0.19	5.3	0.18	0.46	1.0/0.69/0.61
38		>50	>25	0.54	1.9	6.9/3.3/2.3
39		0.15	>25	0.68	0.52	1.8/0.14/0.026
40		33.1	>25	4.6	ND <sup>e</sup>	ND
41		21.4	>25	0.68	1.6	2.4/0.71/0.03

<sup>a</sup> Inhibition of kinase activity (Lantha-Screen).<sup>b</sup> Cell assay measuring p4EBP1 in U87 cells.<sup>c</sup> Cell assay measuring pAKT (S473) in U87 cells.<sup>d</sup> Inhibition of kinase activity (Alpha-Screen).<sup>e</sup> ND = not determined.

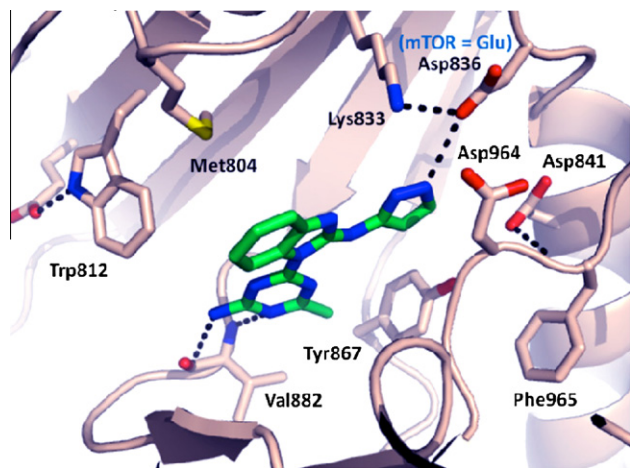


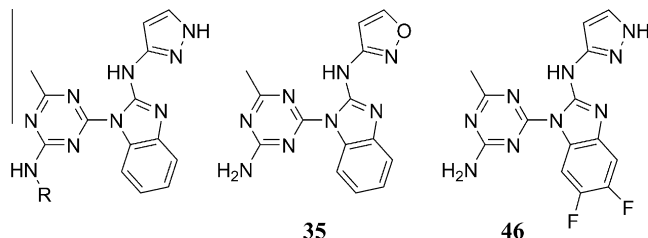
Figure 2. Co-crystal structure of **32** in the kinase active site of PI3K $\gamma$ .

our homology model is the presence of Glu724 in place of the Asp836 present in PI3K $\gamma$ . We reasoned that the additional side chain length of the glutamate, when compared to Asp, could lead to a tighter binding interaction with the pyrazole and also move the lysine closer to the benzimidazole and pyrazole nitrogens. This residue difference could lead to a more effective binding interaction for **32** within mTOR and in turn, impact selectivity over PI3K.

Pharmacokinetic (PK) studies in male Sprague–Dawley rats revealed that **32** demonstrated relatively high clearance ( $CL = 1.9$  L/h/kg), short half-life ( $T_{1/2} = 0.72$  h), poor exposure (IV AUC = 1680 nM h) and poor bioavailability ( $F = 6.3\%$ ). The high clearance observed in vivo was inconsistent with the in vitro intrinsic clearance rates, which were relatively low (79 and 52  $\mu\text{L}/(\text{min mg})$  in human and rat liver microsomes, respectively). Similarly, the in vitro predicted clearance obtained from rat hepatocytes was comparatively low (28  $\mu\text{L}/(\text{min mg})$ ). To further understand the high in vivo clearance, we conducted in vivo metabolism studies by dosing bile duct-cannulated rats with **32**. Using LC/MS analysis, multiple glucuronidation products of both the parent (**32**) and of oxidative metabolites were identified in rat bile (Scheme 2).

To mitigate the oxidation of the benzimidazole ring, bis-fluorinated analog **46** was synthesized and evaluated in vivo in rats. This modification had minimal impact on the potency or selectivity for mTOR, but resulted in an inferior PK profile (Table 3). As an alternative strategy, potential sites of glucuronidation were targeted as a means of reducing the in vivo clearance. The pyrazole in the affinity pocket was addressed first using the isoxazole congener **35**. Although **35** was a much less potent inhibitor of mTOR and exhibited no selectivity over PI3K $\alpha$ , the in vivo PK data was obtained to determine if the pyrazole was the primary site of glucuronidation. No significant improvement in the in vivo clearance, exposure or half life was observed as a result of this substitution.<sup>14</sup> Finally, we examined alkylation of the triazine amine as a means to inhibit

Table 3  
Efforts to improve the PK properties by substitution of the triazine linker-binder



Compd	R	IC <sub>50</sub> (μm)					Rat PK (1 mg/kg IV, <sup>a</sup> 2 mg/kg PO <sup>b</sup> )					
		mTOR	4EBP1	pAKT	P13Kα	P13Kβ/δ/γ	CL (L/h/kg)	Vss(L/kg)	AUC (nM h, IV)	T <sub>1/2</sub> (h, IV)	F(%)	PPB(%)rat
32	H	0.027	0.40	0.055	0.80	0.87/0.51/0.32	1.9	1.1	1680	0.72	6.3	97.2
42	Me	0.081	0.60	0.10	2.2	4.5/0.89/3.2	0.93	0.76	3600	0.56	20.7	99.2
43	CH <sub>2</sub> CN	0.031	0.60	0.073	6.2	8.5/4.0/3.6	2.5 <sup>c</sup>	1.5 <sup>c</sup>	559 <sup>c</sup>	0.45 <sup>c</sup>	0	98.4
44	(CH <sub>2</sub> ) <sub>2</sub> CN	0.060	1.3	0.082	7.7	15.4/5.8/6.2	ND	ND	1020 <sup>d</sup>	0.70 <sup>d</sup>	ND	ND
45	CH <sub>2</sub> CCH	0.080	1.4	0.15	4.0	3.7/4.6/3.7	ND	ND	ND	ND	ND	ND
35	--	0.15	0.33	0.26	0.84	3.1/1.3/2.3	1.8	1.4	1930	0.50	ND	97.7
46	--	0.024	0.34	0.045	0.49	1.0/0.11/0.25	3.0	3.0	964	0.70	6.0	99.0

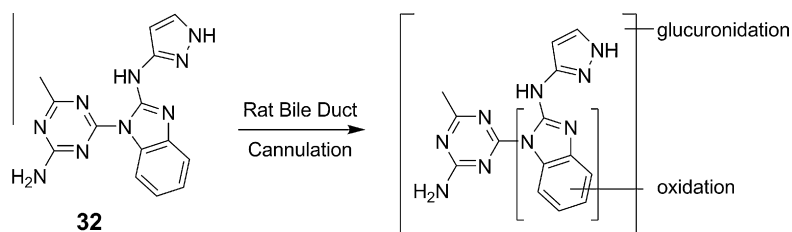
ND = not determined.

<sup>a</sup> Formulation: DMSO.

<sup>b</sup> Formulation: 1% Tween 80, 2% HPMC in water adjusted to pH = 2.2 with MSA.

<sup>c</sup> IV 0.5 mg/kg (DMSO).

<sup>d</sup> Rat PO, 5 mg/kg.



Scheme 2. Metabolites produced from treatment of rats with **32**.

**Table 4**  
Inhibition of proliferation in cancer cell lines by **43**

Cell line	Gene mutation/amplification	IC <sub>50</sub> <sup>a</sup> (μM)
A375	BRAF	0.38
A549	KRAS, LKB1	0.43
BT474	HER2, P13K, p53	0.20
Calu-6	KRAS	0.59
CAL51	P13K, PTEN	0.32
COL0829	BRAF, PTEN	0.34
DU4475	BRAF, APC, RB	0.53
HCC-1954	P13K, p53	0.22
MCF7	P13K	0.54
MDA-MB-231	KRAS, BRAF, p53	0.27
MDA-MB-468	PTEN, EGFR, p53	0.69
NCI-H2009	KRAS, p53, RB	0.42
NCI-H1975	P13K, EGFR, p53	0.60
NCI-H460	KRAS, P13K, LKB1	0.46
NCI-H82	CMYC, RB	0.43
SK-MEL-28	BRAF	0.47
U87MG	PTEN	0.35
UACC-893	HER2, P13K, p53	0.14

<sup>a</sup> Inhibition of proliferation was measured by ATP-lite assay after cells treated with compound for 72 h in 10% serum media; also pictured: Ambit Kinome Scan for **43** at [1 μM]: the red circle on the kinome tree represents TGFBR2 binding. Although tested in the Ambit assay, mTOR and PI3KK are not pictured on the kinome tree.

N-glucuronidation through modification of the electronics or steric hindrance of the triazine amine. Consideration of the SAR developed in Table 1 allowed us to quickly determine which groups would be compatible with maintaining mTOR potency. With regard to selectivity, compound **43** was superior to compounds previously synthesized, showing 200-fold selectivity over PI3Kα, and greater than 100-fold selectivity over the other PI3K isoforms. Additionally, **43** was exquisitely selective for mTOR, showing no

binding to the 402 kinases tested in an Ambit binding assay at [1 μM], with the exception of TGFBR2 (Table 4, POC of 17). Independent testing of **43** against TGFb signaling in a pSMAD cellular assay revealed no significant inhibition of TGFb up to a 10 μM concentration of **43**. The clean kinase profile exhibited by **43** allowed its use as a tool to understand the applicability of an mTOR inhibitor toward various cancer models.

Compound **43** was used to investigate the effect of a selective mTOR inhibitor on a panel of tumor cell lines as a model to predict whether selective inhibition of mTOR kinase activity would have broad efficacy over a variety of tumors. Focusing on melanoma, lung and breast cancer cell lines, compound **43** was tested in a panel of 18 different cancer cell lines of varying mutation status. Sub-micromolar proliferation inhibition was observed upon treatment with **43** in all of the cell lines tested with a mean IC<sub>50</sub> = 0.41 μM. The greatest inhibition was seen in BT474 and UACC-893 breast cancer cells that harbor HER2, PI3K and p53 mutations (Table 4). The efficacy across a variety of cell lines further supports inhibition of mTOR kinase activity as a worthwhile endeavor toward cancer treatment for a broad patient population.

Although compound **43** demonstrated the best potency/selectivity combination, the high rate of clearance and poor exposure observed for this compound precluded further testing in vivo. The analog that provided the most improvement in the PK properties was the triazine methylamine analog **42**. Compound **42** showed slightly diminished potency against mTOR, but maintained the selectivity over the PI3K isoforms when compared with lead compound **32**. Importantly, the installation of the methyl group reduced the in vivo clearance from 1.9 L/h/kg (**32**) to 0.93 L/h/kg (**42**), increased the oral bioavailability by 3× to give F = 21% and improved the solubility (solubility in 0.01 N HCl = 156 μg/mL vs 37 μg/mL for **32**).

Since compound **42** exhibited the most promising combination of potency, selectivity and desirable pharmacokinetic properties, we sought to determine whether it would inhibit mTOR activity in vivo. Before assessing the in vivo pharmacological activity of **42**, it was evaluated against a panel of 100 kinases to determine its selectivity profile. Inhibitor **42** demonstrated excellent selectivity for mTOR and did not significantly inhibit any of the other kinases in the panel, showing only moderate inhibition of YSK4 (POC = 35) and CSNK2A1 (POC = 46) at [1 μM].<sup>15</sup> In order to demonstrate that **42** would inhibit mTOR kinase activity in vivo, a pharmacodynamic assay was conducted to measure the change in HGF-induced phosphorylation of downstream mTOR substrates pAKT and pS6RP (Fig. 3). Inhibitor **42** was administered to mice by intraperitoneal (IP) injection at 10, 30 and 100 mg/kg (N = 3 animals/group).<sup>16</sup> Six hours post-dose, human recombinant HGF was injected intravenously and the livers were harvested. The phosphorylation of AKT (S473, downstream of mTORC2) and S6K (phosphorylation site S240/244, downstream of mTORC1) was measured

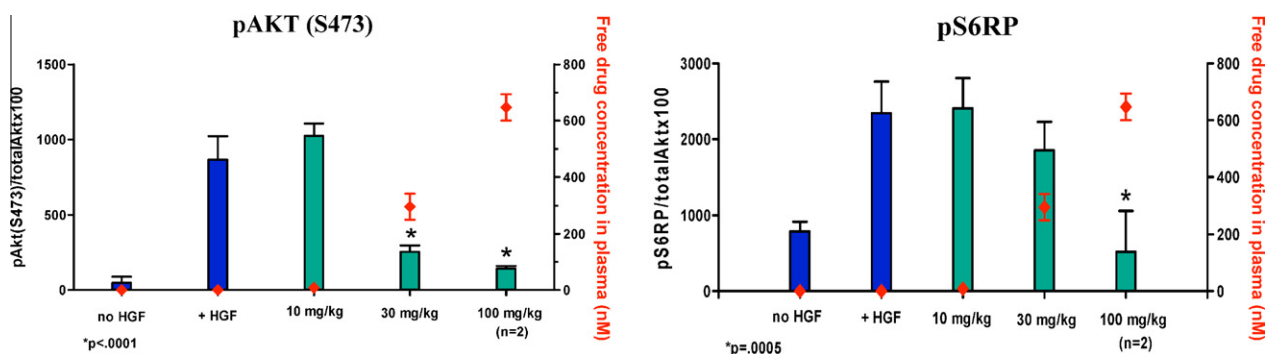


**Figure 3.** Pharmacodynamic assay measuring the changes in of HGF-induced phosphorylation of pAKT and pS6RP in the mouse liver as a result of treatment with compound **42**.

using MSD analysis. Treatment with **42** at 100 mg/kg resulted in significant inhibition of both AKT (83% inhibition,  $p < 0.0001$ ) and S6RP (78%,  $p = 0.0005$ ) phosphorylation in liver tissue at the six hour time point. The mean unbound plasma concentration at the 100 mg/kg dose was 0.65  $\mu\text{M}$ , which was greater than 6-fold over the AKT cellular  $\text{IC}_{50}$  and 1.6-fold higher than the pS6 cellular  $\text{IC}_{50}$  of 0.39  $\mu\text{M}$ . Treatment with 30 mg/kg resulted in a mean unbound plasma concentration of 0.30  $\mu\text{M}$  providing significant inhibition of AKT phosphorylation only (71%,  $p < 0.0001$ ).

In conclusion, by using a combination of targeted SAR with information derived from the X-ray co-crystal structures with PI3K $\gamma$ , novel triazine-benzimidazole mTOR inhibitors were discovered that demonstrated moderate selectivity over the PIKK family of kinases. Although this class of inhibitors suffered from relatively high in vivo clearance and low solubility, compound **42**, which demonstrated the best combination of mTOR potency, selectivity over other kinases and pharmacokinetic properties was tested in vivo in our mouse pharmacodynamic assay. Inhibitor **42** showed dose-dependent inhibition of mTOR kinase activity, showing up to 83% inhibition of downstream substrate pAKT. Additionally, **43** was used as a tool to understand the efficacy profile against 18 cell lines of varying mutation status. Improvements upon this series with regard to potency, selectivity and desirable pharmacokinetic properties will be reported in due course.

#### Acknowledgments

The authors would like to acknowledge Wei Hu, Tisha San Miguel, and Leeanne Zalameda for enzyme and cell assay support. We are also grateful to Loren Berry, Liyue Huang, Meghan Langley, and Jonathan Roberts for PKDM support. Thanks to Jingzhou Liu for metabolite identification studies, Pete Yakowec and Jin Tang for PI3K $\gamma$  expression and purification as well as Huilin Zhao and Linda Epstein for mTOR expression and purification.

#### References and notes

1. Ciuffreda, L.; Di Danza, C.; Incani, U. C.; Milella, M. *Curr. Cancer Drug Targets* **2010**, *10*, 484.
2. Li, Y.; Corradetti, M. N.; Inoki, K.; Guan, K.-L. *Trends Biochem. Sci.* **2004**, *29*, 32.
3. Long, X.; Ortiz-Vegas, S.; Lin, Y.; Avruch, J. *J. Biol. Chem.* **2005**, *280*, 23433.
4. Motzer, R. J.; Escudier, B.; Oudard, S.; Hutson, T. E.; Porta, C.; Bracarda, S.; Grünwald, V.; Thompson, J. A.; Figlin, R. A.; Hollaender, N.; Kay, A.; Ravaud, A. *Cancer* **2010**, *116*, 4256.
5. (a) Rini, B. I. *Clinical Cancer Res.* **2008**, *14*, 1286; (b) Rini, B.; Kar, S.; Kirkpatrick, P. *Nat. Rev. Drug Disc.* **2007**, *6*, 599.
6. García-Echeverría, C. *Bioorg. Med. Chem. Lett.* **2010**, *20*, 4308.
7. Sabatini, D. M. *Nat. Rev. Cancer* **2006**, *6*, 729; Faivre, S.; Kroemer, G.; Raymond, E. *Nat. Rev. Drug Disc.* **2006**, *5*, 671.
8. Chresta, C. M.; Davies, B. R.; Hickson, I.; Harding, T.; Cosulich, S.; Critchlow, S. E.; Vincent, J. P.; Ellison, R.; Jones, D.; Sini, P.; James, D.; Howard, Z.; Dudley, P.; Hughes, G.; Smith, L.; Maguire, S.; Hummersone, M.; Malagu, K.; Menear, K.; Jenkins, R.; Jacobsen, M.; Smith, G. C. M.; Guichard, S.; Pass, M. *Cancer Res.* **2010**, *70*, 288.
9. Barr, S.; Russo, S.; Buck, E.; Epstein, D.; Miglarese, M. AACR 101st Annual Meeting, Washington, DC, 2010, p 1632.
10. Atomic coordinates for the co-crystal structures of **1** and **32** have been deposited in the RCSB with PDB codes 3QAQ and 3QAR, respectively.
11. Knight, Z. A.; Gonzalez, B.; Feldman, M. E.; Zunder, E. R.; Goldenberg, D. D.; Williams, O.; Loewith, R.; Stokoe, D.; Balla, A.; Toth, B.; Balla, T.; Weiss, W. A.; Williams, R. L.; Shokat, K. M. *Cell* **2006**, *125*, 733.
12. (a) Liu, Y.; Gray, N. S. *Nat. Chem. Biol.* **2006**, *2*, 358; (b) Zhang, J.; Yang, P. L.; Gray, N. S. *Nat. Rev. Cancer* **2009**, *9*, 28.
13. Carboxamides as Phenol Bioisostere papers: (a) Breslin, H. J.; Cai, C.; Miskowski, T. A.; Coutinho, S. V.; Zhang, S.-P.; Hornby, P.; He, W. *Bioorg. Med. Chem. Lett.* **2006**, *16*, 2505; (b) Wentland, M. P.; Lou, R.; Ye, Y.; Cohen, D. J.; Richardson, G. P.; Bidlack, J. M. *Bioorg. Med. Chem. Lett.* **2001**, *11*, 623.
14. The in vitro intrinsic clearance was also low for **35** (39 and 46  $\mu\text{L}/(\text{min mg})$ , in HLM and RLM respectively).
15. The custom Ambit 100 kinase binding assay contains a diverse array of kinases from different families and is intended be representative of the wider range of kinases.
16. Although the bioavailability for **42** was improved over **32** and **43**, the oral exposure for **42** did not increase proportional to dose (2 mg/kg PO, AUC = 1490 nM h versus 50 mg/kg PO, AUC = 2030 nM h). From this result it was determined that IP dosing might be the best method to achieve desired target coverage.